Accepted Manuscript

Potential fields modeling of the Serdán Oriental basin, Eastern Mexico

Román Alvarez, Vsevolod V. Yutsis

PII: S0895-9811(17)30220-1

DOI: 10.1016/j.jsames.2017.10.003

Reference: SAMES 1804

To appear in: *Journal of South American Earth Sciences*

Received Date: 29 May 2017

Revised Date: 27 September 2017

Accepted Date: 3 October 2017

Please cite this article as: Alvarez, Romá., Yutsis, V.V., Potential fields modeling of the Serdán Oriental basin, Eastern Mexico, *Journal of South American Earth Sciences* (2017), doi: 10.1016/ j.jsames.2017.10.003.

POTENTIAL FIELDS MODELING OF THE SERDÁN ORIENTAL BASIN, EASTERN MEXICO

Román Alvarez[1] and Vsevolod V. Yutsis[2*]

[1]Instituto de Investigaciones en Matemáticas Aplicadas y en Sistemas, Universidad Nacional Autónoma de México. Ciudad Universitaria, México DF, 04510, México. Ph. +5215554553806; mail: roman.alvarez@iimas.unam.mx

[2]Instituto Potosino de Investigación Científica y Tecnológica, División de Geociencias Aplicadas. Camino a la Presa San José, 2055. San Luis Potosí, S.L.P., 78216, México. Ph. +524448342000; mail: vsevolod.yutsis@ipicyt.edu.m

*Corresponding author: Vsevolod Yutsis (vsevolod.yutsis@ipicyt.edu.mx)

Key words: Maars in Mexico, Monogenetic Volcanism, Axalapaxcos, Modeling of Volcanic Fields, 3-D Inversion of Potential Fields.

ABSTRACT

In the eastern portion of the Trans-Mexican Neovolcanic Belt a group maars, rhyolitic domes, and cinder cones are scattered within the Oriental-Serdán basin. They are flanked by large polygenetic volcanoes. We use aeromagnetic and gravimetric fields to infer and model the main anomalies in the region, with the objective of identifying and characterizing the sub-surface sources of the volcanic activity. A large, positive

magnetic anomaly overlaps the principal area of volcanic activity; it coincides with the main, positive gravimetric anomaly in the area. Both 2-D and 3-D gravity, as well as magnetic models confirm the existence of a large, dense, and magnetized intrusion body nearly reaching the surface, inferred to be the source of the observed anomalies. The intrusion is flanked to the south by rhyolitic domes. Three independently modeled cross-sections coincide in correlating the presence of maars with upward projections of the main intrusion; these projections we interpret as diatreme-type structures, although the modeling scale does not allow for individual identifications. The conduit that supplied magma for the emplacement of the rhyolitic domes of Las Derrumbadas is also identified to depths of four kilometers. A gravity inversion shows in 3-D space the density distribution at various density ranges.

1. Introduction

The Trans-Mexican Neovolcanic Belt (TMNB) extends E-W for over 1000 km in central Mexico. The Oriental-Serdán basin (mean elevation 2400 m) is located on the eastern margin of the TMNB (**Figure 1a**) where a group of rhyolitic domes, maars, volcanic cones, tuffs, and lava flows coexist. The area is flanked by major volcanic structures: Cofre de Perote (4282 m) and Pico de Orizaba (5700 m) the highest summit in Mexico, to the east of the field and Malinche (4461 m), to the west; to the north, lies Los Humeros caldera, a 24 km diameter volcanic structure, where geothermal energy is being exploited. The early inhabitants of the region distinguished between “xalapaxco”, dry crater, and “axalapaxco”, crater with a lake; the latter Nahuatl word is thus equivalent to maar. An

example of an axalapaxco is shown in **Figure 1b**: La Preciosa. Over a century ago Ordoñez (1906) published the first reports on these explosion craters. Bazán (1959) made a geomorphologic, geohydrologic, and geologic description of the basin noting that its drainage has no exterior outlet and rainwater forms shallow lakes and a considerable ground water system, conditions that unquestionably favor phreato-magmatic explosions in the area. A shallow, sandy aquifer named Toba Café contains most of the water that has interacted with magma to produce the explosion craters (Siebe and Verma, 1988; Ort & Carrasco-Núñez, 2009). The distribution of maars and volcanic cones exhibits a roughly N-S trend that parallels the Cofre de Perote-Pico de Orizaba volcanic chain.

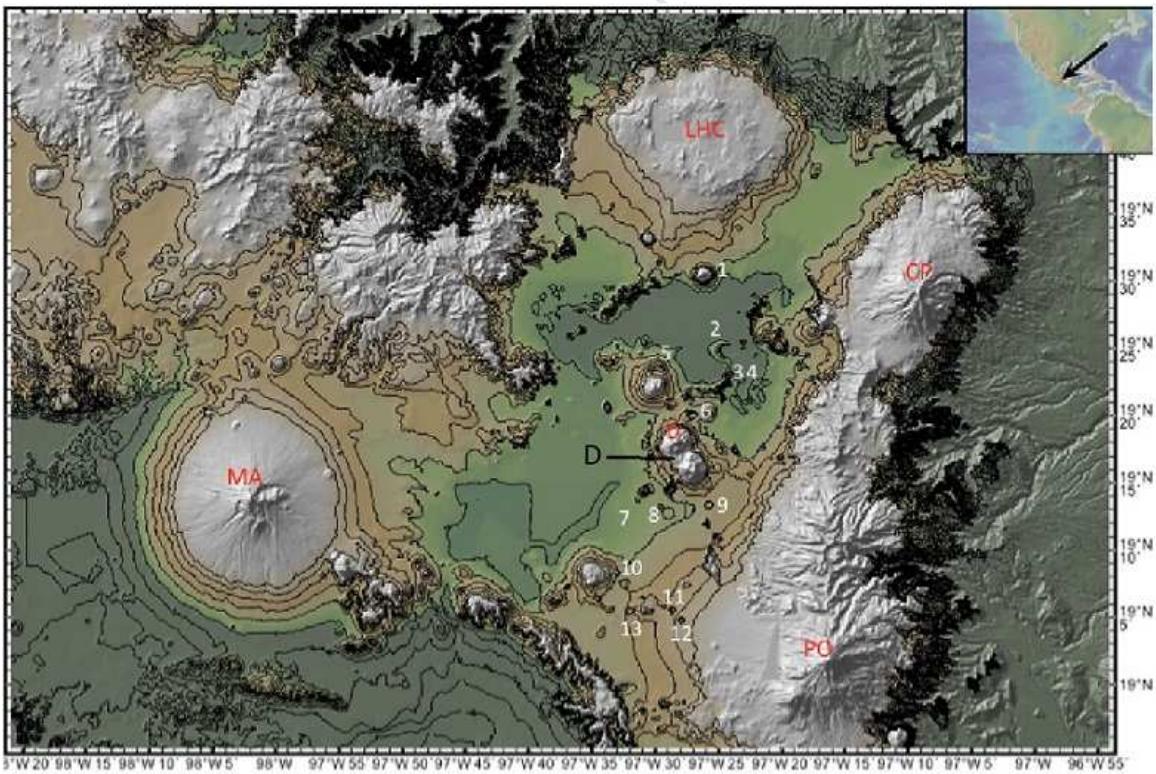

Fig.1a. Oriental-Serdán basin and the distribution of explosion craters. Contours from 2000 to 2250 m in 50 m intervals are shown in black. The lowest elevation

occurs between Las Derrumbadas rhyolitic domes (D) and Los Humeros Caldera (LHC). MA Malinche, CP Cofre de Perote, PO Pico de Orizaba. 1. Cerro Pizarro, 2. Alchichica, 3. La Preciosa, 4. Quecholac ,5. Cerro Pinto (Tepeyahualco), 6. Atexcac, 7. La Hacienda, 8. Buenavista, 9. Tepexitl, 10. Tecuitlapa, 11 Xalapazco Grande, 12. Xalapazco Chico, 13. Aljojuca. Topography from Ryan et al. (2009).

The sources of heat that induce such explosions are ascending rhyolitic magma bodies (Alvarez et al. 1976; Yáñez and Casique-Vázquez 1980; Austin- Eriksson et al. 2011); in two of them, Cerro Pizarro (Riggs and Carrasco-Núñez 2004) and Cerro Pinto, rhyolites have emerged after the explosion took place, since Cerro Pizarro pierces the explosion crater and Cerro Pinto is located on the southern rim of a 3 km diameter explosion crater called Tepeyahualco (Maupomé et al. 1975).

An aeromagnetic survey was flown over several of these structures at elevations above ground ranging from 100 to 300 m in an attempt to establish geophysical criteria to discriminate between the structures (Alvarez et al. 1976). The study concluded that the volcanic cones show the strongest magnetic anomalies resembling a dipolar field, whilst the explosion craters with a tuff ring show weak magnetic anomalies, and collapse structures with no obvious tuff ring may show a strong anomaly, a weak anomaly, or no anomaly at all. Although not the subject of the present study, these early observations of the geophysical character of the volcanic structures involved may help elucidate the subsurface processes that give rise to the molten fuel-coolant interactions and associated diatremes (Lorenz, 1986; Valentine et al. 2012).

Most of the work on the Cuenca Serdán Oriental is focused on the study of the geothermal

potential of the area, especially the Las Derrumbadas domes, or on understanding the bimodal volcanism of the area and linking it to the configuration of the plates underneath it, usually through geochemical studies. We start with a review of previous geological-geophysical studies in this area and make reference to other volcanic studies that have used geophysical surveys to clarify the subsurface nature of such structures.

Siebe and Verma (1988) in their geochemical and tectonic study of the bimodal rocks of the Las Derrumbadas area suggest that this region is of cortical extension characterized by normal faulting and horst and graben structures, where the presence of altered associated fumaroles and rocks indicate an active geothermal system where the immediate heat source is likely to be a reservoir of shallow silica magma. For the genesis of volcanic materials in the Las Derrumbadas area, the presence of compositional voids suggested that siliceous rocks are derived from the partial melting of crustal rocks by intrusion of basalt magmas derived from the mantle. Ferriz and Mahood (1986) studied the implications of the volcanism in the TMNB; they focused on the domes of the Serdán-Oriental Basin. They were described as domes of rhyolitic composition with high content of silica, whose volumes vary between 1 and 5 km^3, the domes are distributed in an area of approximately 300 km^2, and show a rough north-south alignment.

One of the first geological models of caldera Los Humeros in context with the geothermic conductive regime was realized by Prol and González-Moran (1982). They proposed that at depths of 1 to 3 km a layer exists with a high porosity which permits fluid circulation and induces deformation of the isotherms. Gómez-Tuena and Carrasco-Nuñez (2000) described

the Cerro Grande volcano as a well-preserved compound volcano with a low angle that evolved between 11 and 9 Ma. It represents the beginning of volcanism in the eastern sector of a young TMNB. Its extensive stratigraphic and petrological work revealed a complex volcanic evolution that can be summarized in six main stages. The shallow structure of Los Humeros and Las Derrumbadas geothermic fields was studied by Campos-Enríquez and Garduño-Monroy (1987). They have shown a regional weakness zone (the Libres-Oriental depression), where the volcanic activity related to the geothermal manifestation took place. A number of studies were concerned with the magmatic and tectonic aspects of the TMNB in general. Here we only refer to Ferrari et al., (1991) and Ferrari et al., (2005). These authors show the relationship between Cenozoic volcanism of the TMNB, the geological structure of the different volcanic fields and the geothermal regime.

Geological-geophysical studies of monogenetic volcanism are well-known in different parts of the world. A complete description on this theme is presented in Németh et al. (2012) for monogenetic volcanism of the South Aucklend volcanic fields in New Zealand. These authors define different forms of individual volcanoes as scoria cones, tuff rings, maars or tuff cones. They indicate that a common problem of the study of young volcanism is the lack of datable material. Geophysical evidence for structural and spatio-temporal relationships for the Aucklend volcanic field are described by Cassidy and Locke (2010).

Paoletti et al. (2009) carried out a geophysical study of high-resolution aeromagnetic and self-potential (SP) fields and realized a joint modelling of the magnetic and gravity data of

the active volcanic region in the Southern Italy. The 2-D joint forward modelling over Mt. Epomeo (Ischia volcanic island) showed a strong gravity and a SP positive anomaly, while the observed magnetic field revealed a large negative anomaly. Authors explain this phenomenon by the presence of pyroclastic products and trachytic intrusions into the Epomeo and Trippodi mountains. The distribution of basaltic volcanism on Tenerife (Canary Islands) was described Geyer and Martí (2010). They investigated implications of these volcanic processes on the origin and dynamics of rift systems.

Another example of geophysical modelling of the volcanic structures may be found in 3-D gravity inversions, carried out by Blaikie et al. (2014) interpreting subsurface structures in Southern Australia. They studied maar volcanoes using potential field and petrophysical data. Their models show that free-air gravity, and magnetic fields reduced to the pole, were best fitted for the Ecklin maar, Lake Werowrap, Red Rock Volcanic Complex, and Mount Leura Volcanic Complex.

In this study, rather than focusing in modeling the details of individual maar structures by geophysical means (Mrlina et al. 2009; Whiting, 1986; López Loera et al. 2008), we are interested in describing the collective existence of various volcanic structures in the study area and some physical properties of their substrate, which is the intrusive enveloping them. This intrusive is suspected to be the common source of heat that gives rise to the observed magmatic and phreatomagmatic surface volcanic manifestations. In order to do this we use gravity and magnetic fields and build 2-D models and 3-D inversions of these fields.

Fig. 1b. La Preciosa maar. An example of the 'axalapaxcos´ (local word for maars) present in the area. In the background some of the region's cinder cones (arrows). The dashed line along the lake's shore indicates the contact between the tuff ring and the country rock.

Obtaining the 3-D characteristics of the sources of the anomalies in volcanic fields by means of direct inversion techniques is gaining momentum (Montesinos et al. 2005; Blaikie et al. 2014; Alvarez and Yutsis, 2015; Alvarez et al. 2017 a,b). As a coherency test between the 2-D and 3-D models we superpose and compare cross-sections obtained from the 3-D models to the sections modeled in 2-D.

2. Regional Geology

In the region, one finds outcrops of igneous, sedimentary, and metamorphic rocks. The oldest igneous and metamorphic formations representing the regional basement, are gneiss and biotite-schists of Permian-Jurassic age and tonalities of Jurassic-Cretaceous age (Lira, 2005; Gutierrez-Negrín, 2015) outcropping towards the north of the region. On top of some of them lay continental sedimentary rocks of the Upper Triassic and Lower to Medium Jurassic, while in other areas they are covered by marine sedimentary rocks of the Upper Jurassic and the Cretaceous. Volcanic activity throughout most of the region initiated in the Miocene, around 10 Ma ago, and continued in the Pliocene between 3.5 and 1.9 Ma (Gutierrez-Negrín, 2015; Yáñez and Casique-Vázquez 1980). The youngest Quaternary volcanism is basaltic to basaltic andesite, with rhyolitic components (Ort and Carrasco-Nuñez, 2004; 2014).

In **Figure 2** a geologic map of the area is presented where we have highlighted the presence of explosion craters, with and without lakes, lava flows and scoria cones all with a basic composition, mostly olivine and pyroxene basalts (Qvb), and Quaternary alluvial deposits (Qal). In the area close to the Las Derrumbadas ryholitic dome-complex (Qrio), this volcanism is prevalent on both sides of the domes with a NW-SE orientation. Las Derrumbadas system initiated along various deep, NW-SE fractures that gave rise to the emission of andesitic, rhyolitic and basic magma. These fractures gave rise to several structures of the fissure type in the southern part. In the central part, the rhyolitic system of Las Derrumbadas and Cerro Pinto domes was emplaced, while in the north, numerous scoria cones appeared, some of them with associated lava flows. A fissural flow of the domes represents the last active stage around Las Derrumbadas, probably the result of a re-

activation of their magmatic chamber; its composition varies between dacitic and andesitic. In **Figure 2** we have included the presence of an inferred normal fault encompassing the NW alignment of nine structures, from SE to NW they are: Xalapazquillo o Tepexitl, the two rhyolitic domes of Las Derrumbadas, two scoria cones, Atexcac maar, Cerro Pinto rhyolitic dome, the neighbour explosion crater, and Xalapazco del Barrio. We submit that the alignment of these structures is caused by the weakness zone generated by the fault.

The most recent activity is represented by the presence of numerous explosion craters in the area; some of them have been previously reported from geophysical or geological viewpoints. Tepexitl is a rhyolitic tuff ring (Austin-Eriksson et al. 2011) located SE of Las Derrumbadas domes, aligned with them and with Cerro Pinto to the NW. It was originally proposed to be of meteoritic origin (Maupomé et al. 1975) and subsequently characterized geomagnetically (Alvarez et al. 1976).

Additional dome structures of the rhyolitic type are found at Cerro Pinto, and Cerro Pizarro. Yáñez and Casique-Vázquez (1980) proposed that these domes appeared throughout the area at the end of the igneous episode. They were emplaced as highly viscous bodies, taking advantage of the previous emission conduits of older materials, blocking them in all cases. This is confirmed by the inability to find the sources of pre-existing flows. In particular, the magma of Las Derrumbadas has no evidence of flow or ductile behaviour; it rose to the surface in a very slow way and almost as a solid body, carrying upwards a large amount of pre-existing materials, which subsequently have been eroding easily, giving rise

to landslides (derrumbes) and lahars.

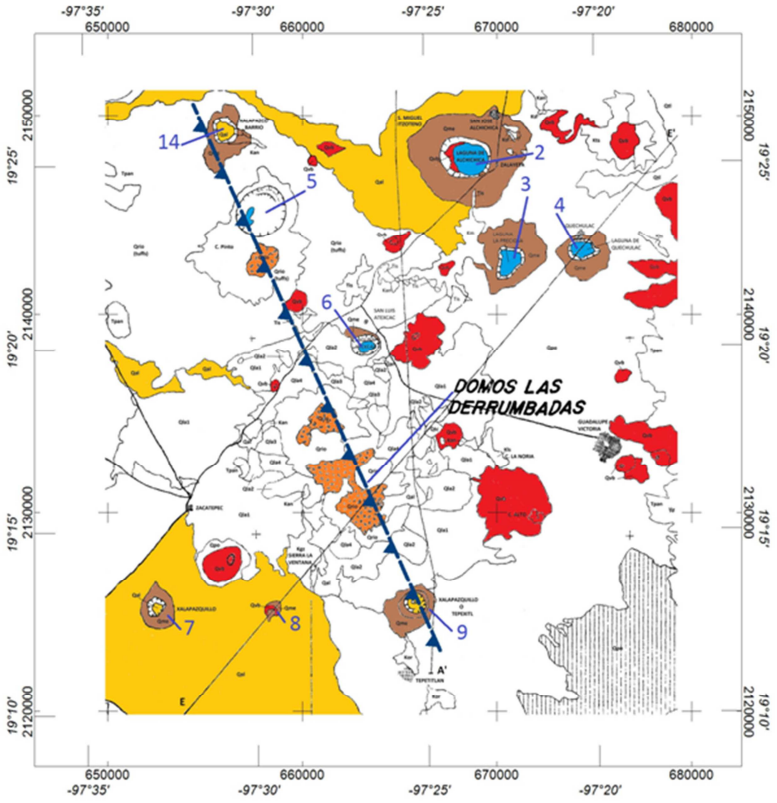

Fig. 2. Geologic map modified after the unpublished report of Yáñez and Casique-Vázquez (1980). Structures are numbered according to those in Figure 1a; 14 corresponds to Xalapazco del Barrio. Quaternary structures relevant to the present study are shown in color. An inferred, SE-NW trending fault links nine of these structures. Qal, alluvium; Qvb, basic volcanism, basalts and scoria; Qme, materials from explosion craters, ashes of basic composition; Qrio, rhyolites, ryholitic tuffs, traquite and latite.

3. Magnetic field

The aeromagnetic map NAMAG (2002) of the area was reduced to the pole (Baranod and Naudy 1964) and is shown in **Figure 3**. A prominent WNW trending set of magnetic positive anomalies divides the area. A set of magnetic negative anomalies runs parallel to

the S the whole of its length. A good correlation is observed between positive magnetic

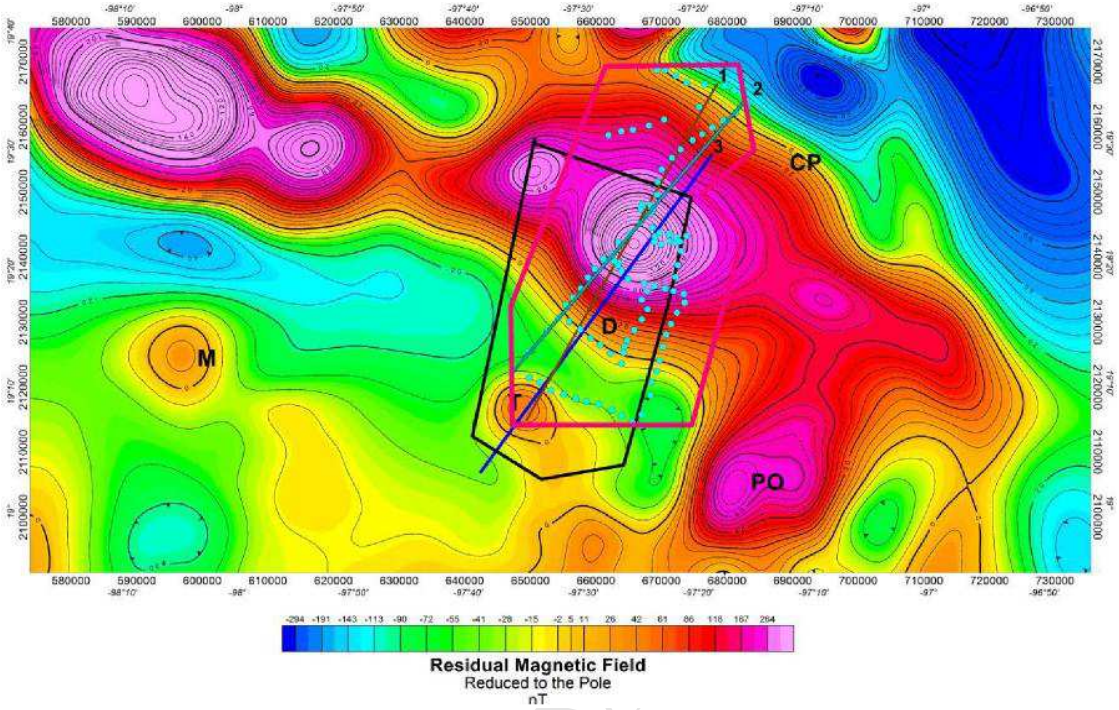

Fig. 3. Regional, residual magnetic map from NAMAG (2000) reduced to the pole. Contour interval is 20 nT. There is a prominent NW trending set of positive magnetic anomalies. The magnetic high near the center of the figure encloses most of the volcanic structures in Las Derrumbadas (D) area. Line 1 corresponds to the magnetic cross-section presented ahead. Line 2 corresponds to the gravity cross-section. Line 3 shows the location of the magnetic 2-D model. The five-sided polygon corresponds to the area selected for the 3-D magnetic inversion, while the eight-sided polygon corresponds to the area selected for the 3-D gravity inversion. T - Tecuitlapa volcano, M - Malinche, CP - Cofre de Perote, PO - Pico de Orizaba.

anomalies and outcropping volcanic structures. The magnetic positive anomaly close to the center coincides with most of the explosion craters and scoria cones in the northern portion of the area. To the south of it, a negative magnetic anomaly separates another group of explosion craters and volcanic cones (Aljojuca and Tecuitlapa fields) associated with a corresponding, smaller, positive magnetic anomaly. **Figure 4** shows the

topographic map of the area, with the magnetic contours of **Figure 3** superposed, which makes it easy to observe the direct correlation between them.

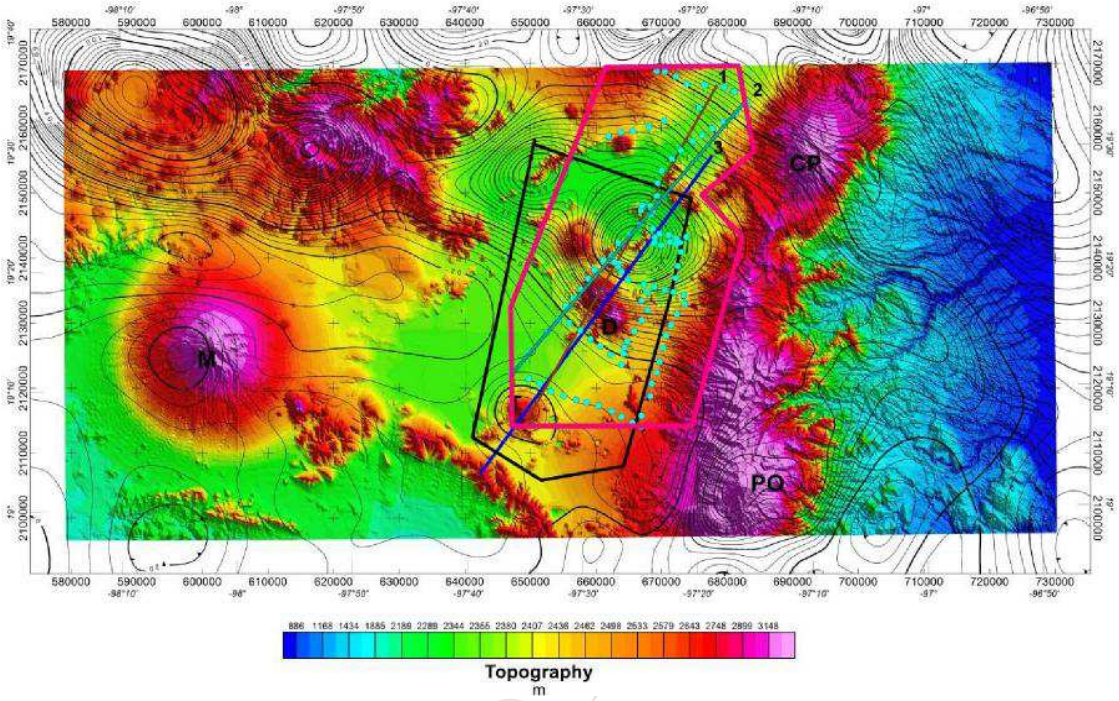

Fig. 4. Topographic map of the area from Ryan et al. (2009). Contours are reproduced from those of the magnetic field in **Figure 3**. Gravimetric station locations are shown as blue dots. Line 1 corresponds to the magnetic cross-section presented ahead. Line 2 corresponds to the gravity cross-section. Line 3 shows the location of the magnetic 2-D model. The five-sided polygon corresponds to the area selected for the 3-D magnetic inversion, while the eight-sided polygon corresponds to the area selected for the 3-D gravity inversion.

To explore probable occurrences and distribution of magnetized bodies along Line 3 (**Figure 3)** a 2-D model was constructed, shown in **Figure 5**; the line crosses Tecuitlapa volcano, Las Derrumbadas rhyolitic domes and the maximum of the central magnetic anomaly. Pertinent magnetic susceptibilities are assigned to the proposed geologic formations in order to reproduce the measured magnetic field.

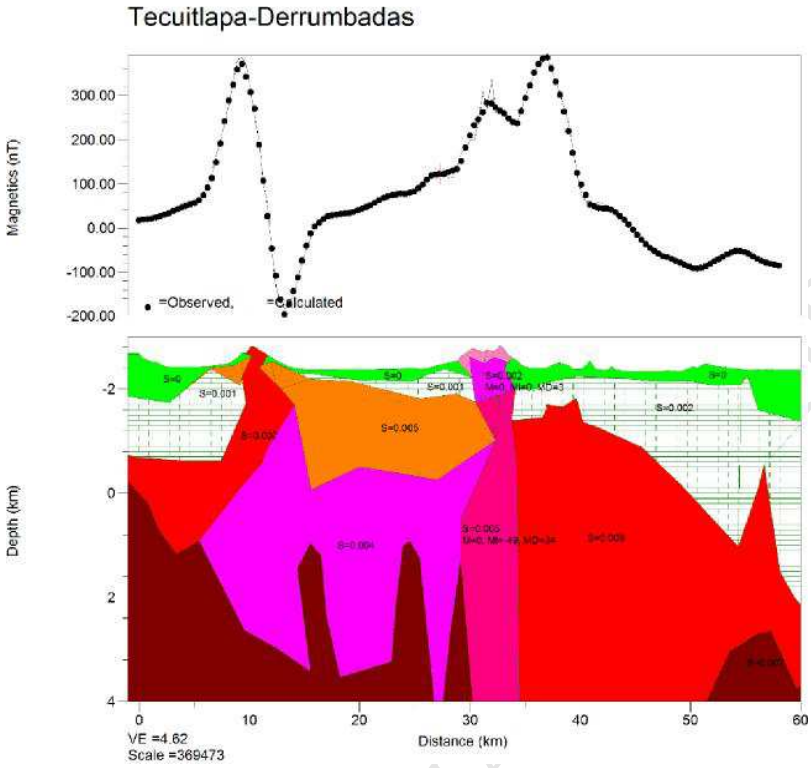

Fig. 5. Magnetic field model along Line 3 (**Figure 3**). High magnetic susceptibility bodies (red) are located close to, or reach the surface at Tecuitlapa volcano (x=11 km) and Las Derrumbadas domes (x=32 km). Associated magnetic susceptibility values (emu) are shown for each formation.

Volcanic sediments, limestone formations, rhyolites and igneous intrusions are represented in the model, which confirms that the main intrusive gives rise to the large magnetic anomaly appearing in **Figure 3.** Las Derrumbadas domes are on the edge of this body to the south probably correspond to the NW-SE fault system described by Yáñez and Casique-Vázquez (1980). Through this channel basic and dacitic/andesitic flows have been emplaced at the surface. The model is consistent with high-susceptibility materials being extruded at the surface at this location. To fit the observed field only the formation

associated with Las Derrumbadas requires some remnant magnetization.

A narrow conduit extends vertically from Las Derrumbadas domes (x=34 km) to a depth of 4 km, corresponding to the inferred normal fault in Figure 2. In the model, to the north of Las Derrumbadas a large intrusive body is located that most likely is the source of heat for the phreatomagmatic explosions observed in the area. In the southern portion of the transect the model shows another high-susceptibilty body reaching the surface at the location of Tecuitlapa volcano. From the geologic description we know this body is of a different composition from that of Las Derrumbadas (Ort and Carrasco-Nuñez 2014). The sources of magma for the two bodies reaching the surface have to be different and separated from each other since they have different compositions: Las Derrumbadas is acidic while Tecuitlapa volcano is basic in composition.

4. Gravity field

The gravity field was measured at 104 stations whose locations appear in **Figure 4**. Measurements are distributed mainly around Las Derrumbadas area; the Tecuitlapa-Aljojuca field is not included in this analysis. The residual Bouguer anomaly is presented in **Figure 6**. This residual anomaly was obtained from the complete Bouguer anomaly subtracting the regional field, which was obtained with a second degree polynomial.

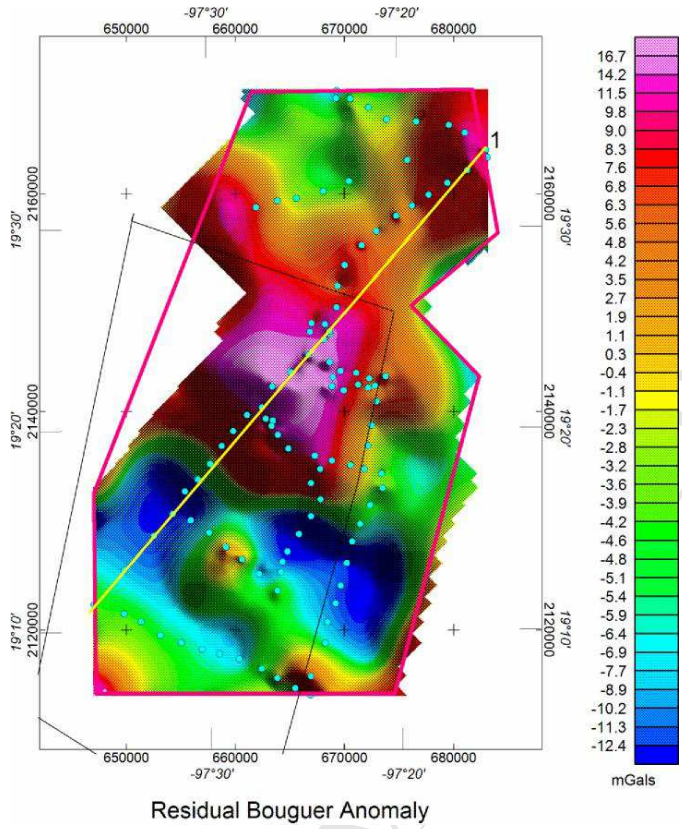

Fig 6. Gravity field was measured at the station locations (blue dots); a second-degree polynomial representing the regional field was subtracted in order to obtain the residual Bouguer anomaly and subsequently interpolated with a minimum curvature algorithm. The central, positive anomaly corresponds directly with the location of the positive magnetic anomaly in **Figure 3**. The straight line labeled 1 locates the density cross-section derived from the 3-D inversion. The eight-sided polygon is the area where the 3-D gravity inversion was performed. The cropped polygon corresponds to the region in which the magnetic inversion was performed

The gravimetric positive anomaly is located between Las Derrumbadas and Tepeyahualco explosion crater and correlates closely with the large, positive, magnetic anomaly described above, suggesting that both anomalies, magnetic and gravimetric originate in the same intrusive body. This is actually confirmed by the 2-D gravity model (**Figure 7**) calculated along Line 2 (**Figures 3, 4**).

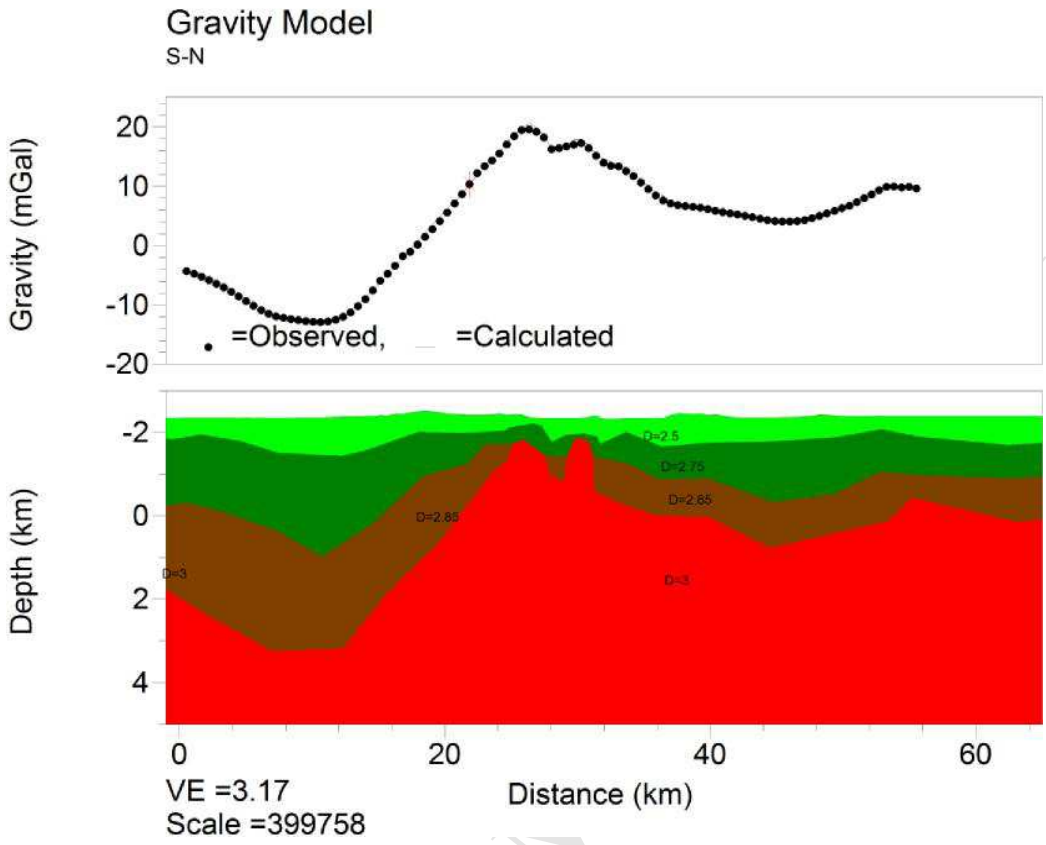

Fig.7. 2-D gravity model along Line2 in **Figures 3 and 4**. The formation of density 3.0 g/cm^3 rises approaching the surface, closely corresponding to the magnetized body shown in the 2-D magnetic model of **Figure 5**.

The model reaches 5 km depth; it shows a dense body (3.0 g/cm^3) rising to the surface in the region of the explosion craters. Lower density formations overlie the intrusive body originate in the same intrusive body. This is actually confirmed by the 2-D gravity model (**Figure 7**) calculated along Line 2 (**Figures 3, 4**). Las Derrumbadas domes are located at x=18 km, on the south side of the rising intrusive body. When comparing the 2-D magnetic and gravimetric models, we find that both support the existence of the intrusive body located close to the surface in the explosion craters' region and both

suggest the presence of two, smaller protruding intrusions, which coincide with the location of maars and explosion craters at the surface.

5. 3-D magnetic and gravity inversions

In order to perform a 3-D inversion of the gravity or magnetic fields we use the inversion method described by Macleod and Ellis (2013), based in turn in the theoretical considerations of Ellis et al. (2012); the magnetic inversion takes into account remnant and induced magnetizations. A 3-D mesh is built under a selected surface area in which a grid of magnetic or gravity values is defined. In the present case, the selected surface areas are delimited by the polygons shown in **Figure 3**. Each volume element (voxel) of the mesh is assigned a density or a magnetic susceptibility value, depending on the type of inversion performed. Next, the contribution to the total field of each voxel is calculated at an observation point on the surface. The total contribution of the set of voxels is compared to the corresponding measured value at the surface. Densities or magnetic susceptibilities are modified, and the process is repeated for each observation point at the surface until the difference between the calculated and measured values is less than a predetermined value. In our case, this value was chosen to be 5 percent of the standard deviation. Thus the grid generated by the inversion process does not differ from the measured grid by more than 5 percent of the standard deviation. In the present inversions, grid dimensions within the five-sided polygon in Figure 3 are 37 x 56 x 10 cells of X=1, Y=1, and Z= 0.925, 0.856, 0.793, 0.734, 0.680, 0.629, 0.583, 0.540, 0.500, and 0.500 km respectively. As can be seen, the cell height Z is variable, with

the smaller cell sizes at the top layers. This was done to bring the model to best fit in accordance with the VOXI modeling.

Results of the 3-D magnetic field inversion are shown in **Figure 8a** and **b**. Both show the prisms' distribution and are clipped to the east along Line 2 (**Figures 3 and 4**), within the extent of the reference polygon. In **Figure 8a** the distribution is shown in an ample range encompassing negative susceptibilities through to the highest positive values. High susceptibility values correspond to the location of the Tecuitlapa structure and the region north of Las Derrumbadas domes, or the main intrusive body. The lowest susceptibility region corresponds well with the faulted region south of Las Derrumbadas domes. This region, however, does not extend to the surface as might be expected, since the fault does appear at the surface. It starts at a depth of sea level and continues to deeper levels. The region above it shows larger susceptibility values representing Pliocene-Quaternary volcanic rocks that, as can be appreciated from the model, practically cover the whole region. In **Figure 8b** the distribution has been clipped as to show only the distribution of the highest susceptibilities (+0.0006 to +0.0076 SI). Tecuitlapa and the main intrusive body, including Las Derrumbadas, appear isolated from each other; the main body exhibits the largest magnetic susceptibilities down to the -3 km level. Whilst the model of the main body shows spherical geometry, Tecuitlapa structure is elongated towards the east. We recall that it is in that direction that Aljojuca, Xalapaxco Grande, and Xalapaxco Chico are located, as well as the Zotoltepec scoria cones, suggesting a causal relationship between this elongated structure and the surface presence of volcanism.

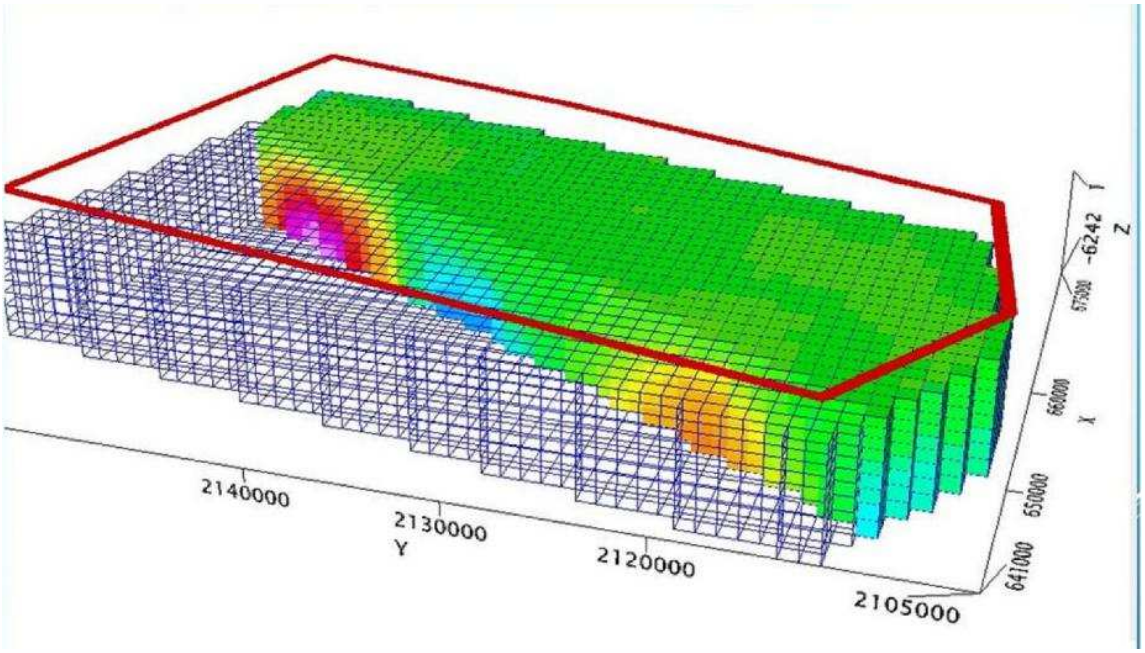

Fig. 8a. Inverted magnetic susceptibility distribution clipped along Line 2 (**Figures 3 and 4**) and in the -0.0036 to +0.007 SI range. Magenta corresponds to the highest values and blue to the lowest. The reference polygon for the inversion as well as the mesh are shown. The high susceptibility region to the south corresponds to Tecuitlapa volcano, while the one to the north corresponds to Las Derrumbadas region. The faulted region is shown in blue

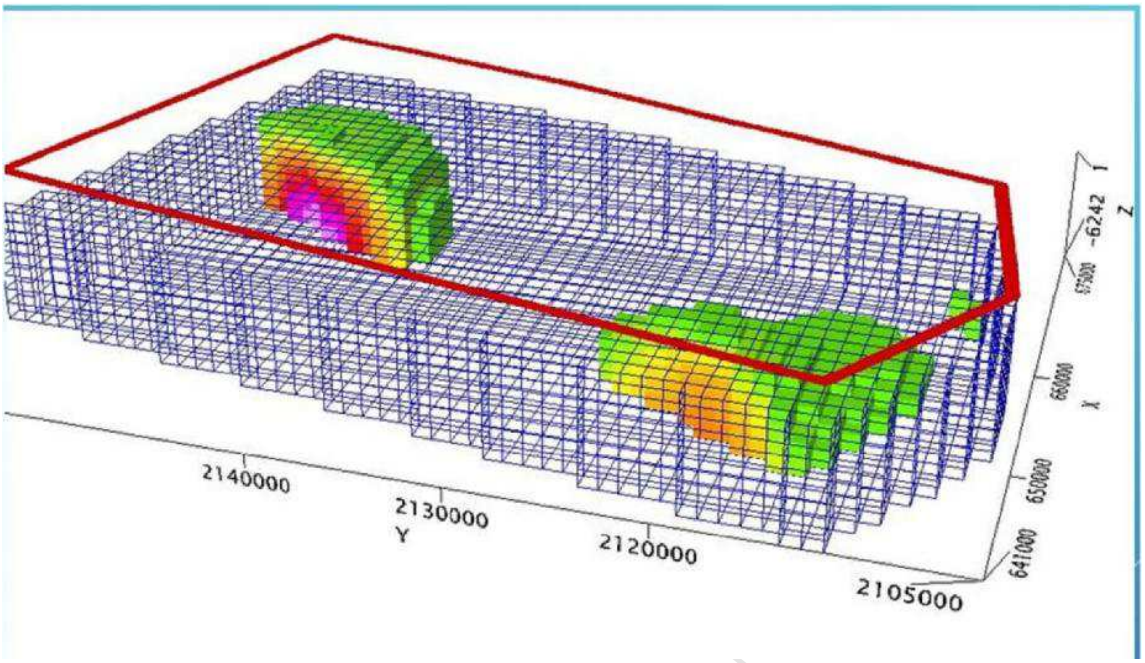

Fig. 8b. Inverted magnetic susceptibility distribution clipped along Line 2 (**Figures 3 and 4**) and in the +0.0006 to +0.0076 SI range. Magenta corresponds to the highest values and green to the lowest. It shows the reference polygon and the mesh used for the inversion.

The 3-D inversion of the gravity field yielded the density distribution shown in **Figure 9**, showing the overall inverted volume. The density distribution can now be analyzed selecting density ranges of interest. In **Figures 10a** through 10**d** results are presented with various depth and density ranges. They illustrate how in the present case, the density distribution evolves from dense cores to the low density materials of the surrounding formations. **Figure 10a** shows the distribution of materials in the 2.69 - 2.88 g/cm^3 density range within the inverted volume.

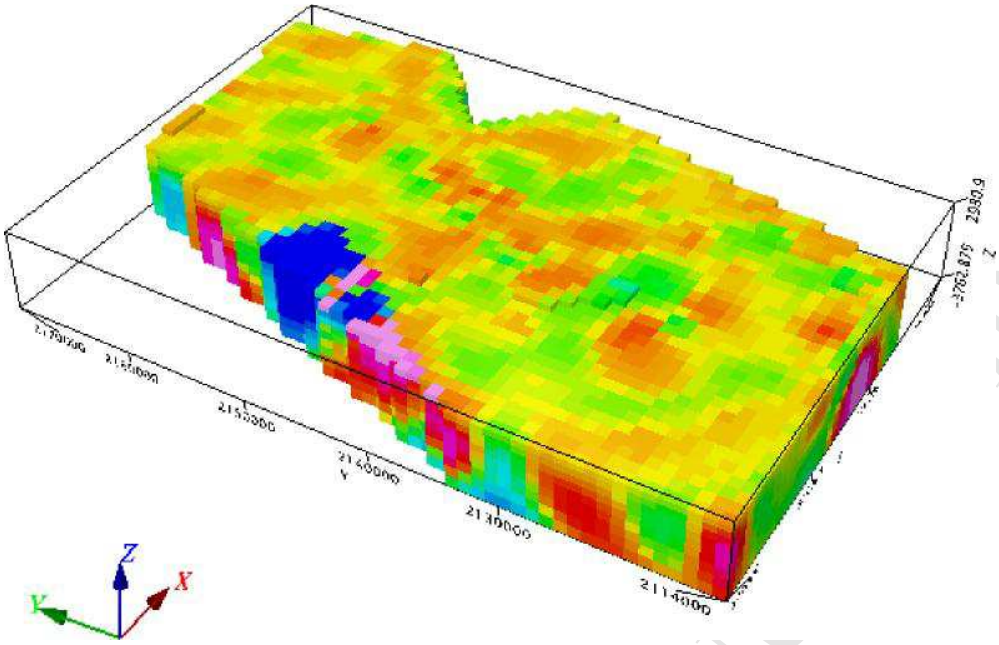

Fig. 9. 3-D inversion of the gravity field showing the density distribution in the volume under the corresponding polygon in **Figure 3**. Although the reference polygon over the model is not shown it can be easily inferred. Actual densities can be obtained adding the reduction density (2.67 g/cm^3) to the values in the colour scale.

Also shown are the reference polygon delimiting the area of the inversion, as well as L1, the line corresponding to the 2-D gravity model along which a density cross-section derived from this inversion will also be presented, and the location of the NW trending fault system (F) reported by Yáñez and Casique-Vázquez (1980). At the scale of the model, the conduit feeding Las Derrumbadas appears attached to the main intrusive body. Meanwhile the fault region appears as low-density, showing an empty region in the density range analyzed, thus coinciding with the low magnetic susceptibility illustrated in **Figure 8a**. We notice again the coincidence of the central intrusive body with the region

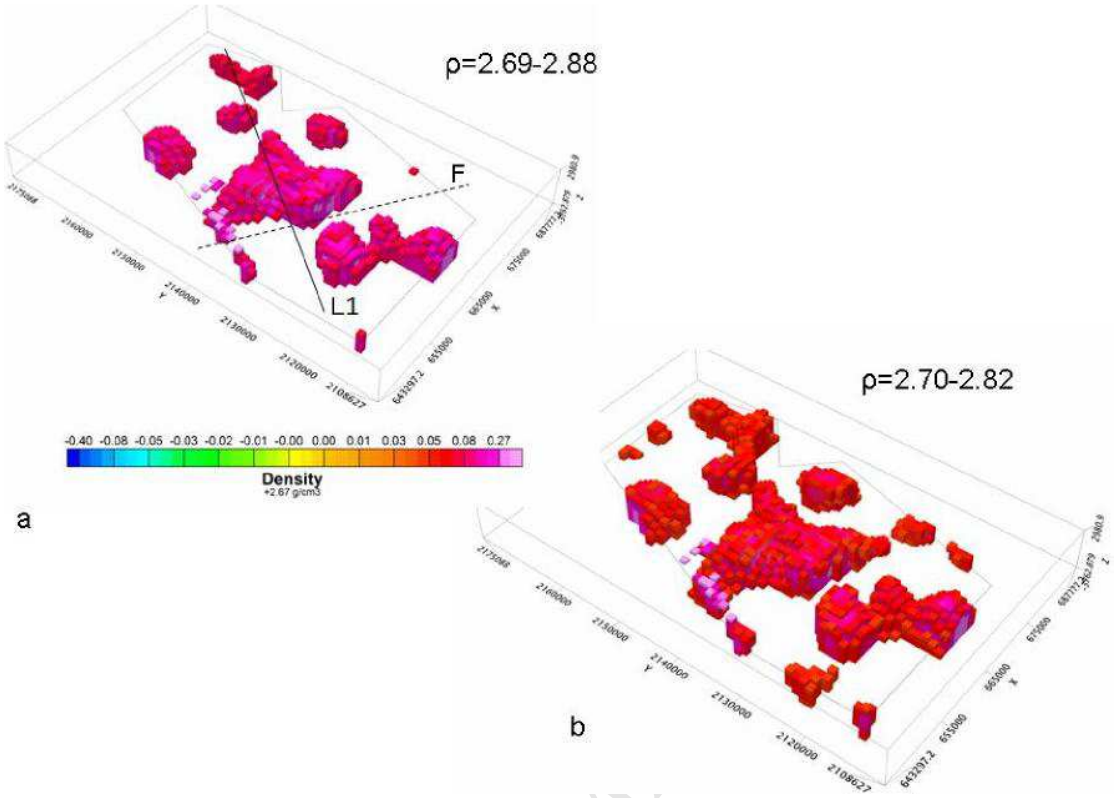

Fig. 10. a) Density distribution clipped to show only the 2.69-2.88 g/cm^3 range. The reference polygon is shown, as well as the traces of line L2 and fault F. In order to obtain actual densities one must add the reduction density (2.67 g/cm^3) to the values in the color scale. b) Density distribution clipped to show the 2.70-2.82 g/cm^3 range. Lower densities add to the previous range increasing the observed volume towards the surface. The color scale is the same as that of **Figure 9**.

of surface explosions; the area corresponding to Tepeyahualco and Cerro Pinto correlates with an extension to the NW of this body. In the NW portion of the reference polygon a further dense isolated intrusive body corresponds with the position of Cerro Pizarro, indicating that there too the local volcanic activity was induced by a dense intrusive approaching the surface. These observations suggest a causal relationship between the explosion craters observed on the surface and the distribution of the denser

formations in the model. However, this represents only one requirement for the phreato-magmatic explosion to occur, the other requirement is the presence of water contained in an aquifer, which in this case is the Toba Café formation. The only exception appears to be the dense body south of the fault (F) and east of L1 that has no explosion craters associated; in the surface this region corresponds to a plain extending between Tecuitlapa volcano and Las Derrumbadas domes. However, when compared with the magnetic model of **Figure 4** two bodies of high magnetizations are found at depths between -2 and 3 km, which probably correspond with the high-density body. This region deserves a more detailed study to determine its present state of activity.

Figure 10b shows a lower density interval (2.70-2.82 g/cm^3) whose elements begin to cover the high-density region presented in **Figure 10a**. The density ranges were selected during modeling taking into account the best fitting of observed and calculated gravity data. Note that the main intrusive is elongated in the SE-NW direction; the NW tip of this body lies underneath Tepeyahualco and Cerro Pinto maar. We observe that the center of the main intrusive body projects markedly towards the surface evoking dike injection and the formation of a diatreme in that direction. The fault zone appears devoid of materials in this density range. **Figure 10c** shows the distribution of materials in the 2.68-2.80 g/cm^3 density range within the area of inversion. Materials in this density range continue to grow upwards covering the denser formations.

Figure 10d is the same as the distribution in **Figure 10c**, except it is clipped at an

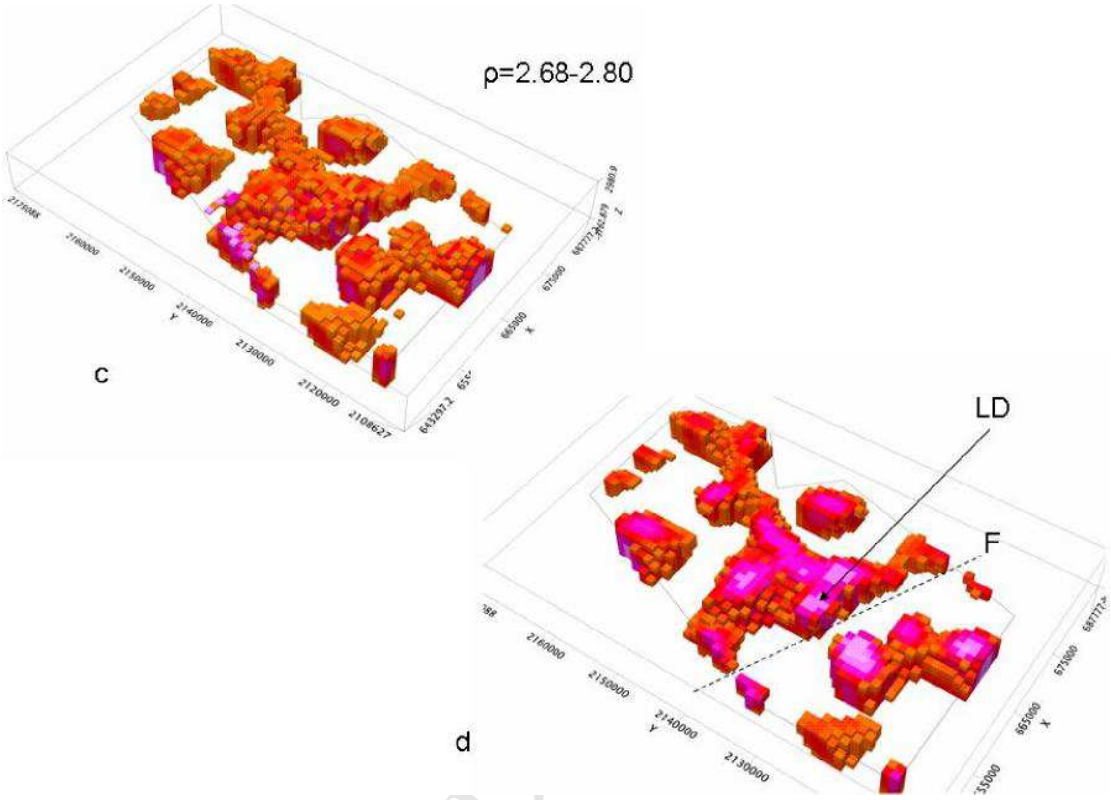

Fig.10. c) Density distribution clipped in the 2.68-2.80 g/cm3 density range. d) The density distribution in **Figure 10c** is now clipped in the z-direction between depths of 830 and 3500 m below sea level. LD Las Derrumbadas conduit. F Fault.

elevation interval between 830 and 3500 m in order to observe the density distribution at the former depth. At the top of this distribution (830 m below mean sea level) we identify Las Derrumbadas conduit as closely associated with the southern section of the main intrusive body, suggesting that the conduit was fed by this body. The distribution of the highest density regions displays two main orientations: a NW-SE

orientation and what appears to be a secondary, perpendicular orientation, placing Las Derrumbadas conduit at their intersection.

From the inverted density distribution we extracted the vertical cross-section along L1 (**Figure 11**), which can be compared with the 2-D models in **Figures 6** and **7.** Performing these comparisons one must bear in mind that in the 2-D magnetic models the boundaries between density contrasts are sharp, while in the cross-section the prisms' densities are interpolated appearing as smooth changes. A central, high-density region dominates to depths of 4 km and corresponds to the main intrusive body. The highest densities appear in the depth range of 1 to 4 km. We note the irregular character of the uppermost layers of this body, noting that two branches approach the surface, coinciding with the location of two maars: Atexcac and Alchichica. Similar irregularities are observed in the 2-D models defined above. This result again supports the previously made assumption that these branches probably represent the magma pathways that interacted with aquifers inducing the explosions and forming diatremes and maars.

The upper portion of this figure shows the topographic profile along the line, where the position of Las Derrumbadas and the two explosion craters are indicated. Las Derrumbadas extrusive bodies limit the extension of the dense intrusive body to the SW. From the density cross-section (**Figure 11**) and the 2-D magnetic susceptibility model (**Figure 5**) we infer that the extrusion region for these domes is limited by two high-angle faults. Thus, these rhyolites appear to have been channeled upwards by the same tectonic forces that emplaced the main intrusive body, taking advantage of a weakness zone. These

rhyolitic domes still exhibit fumaroles.

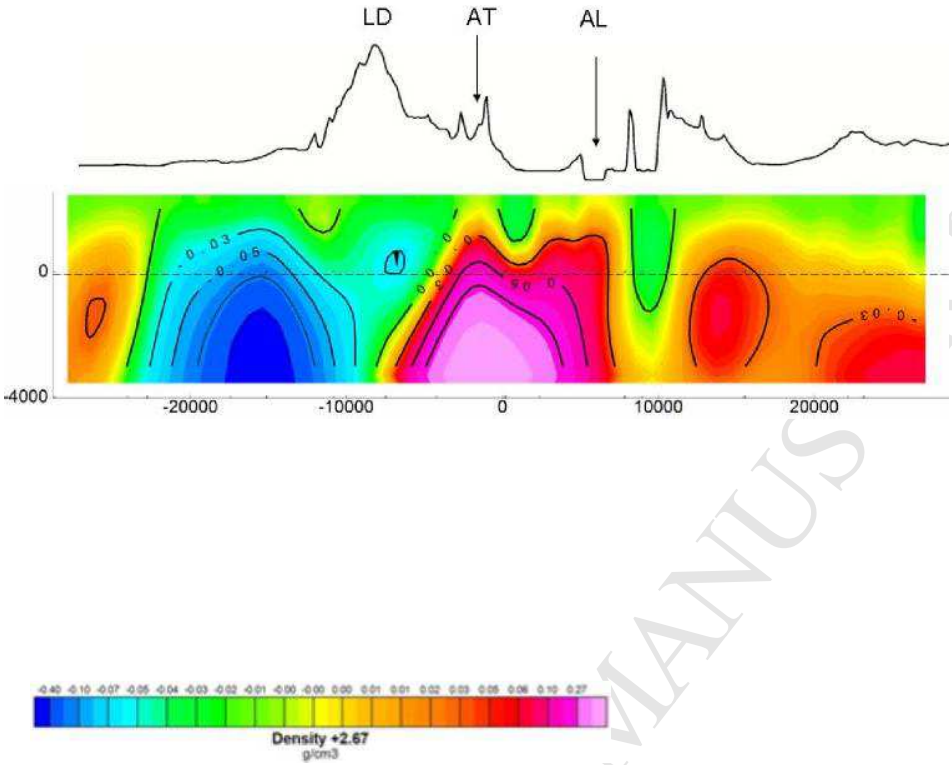

Fig. 11. Cross-section of the inverted gravity field along Line 2 in **Figures 3 and 4**. Again, the actual density values are obtained adding the reduction density (2.67 g/cm^3) to density values in the scale. Scales in X and Z axes are in meters. The central positive anomaly corresponds to an intrusive body whose maximum density occurs between 1 and 4 km depth. The dashed line represents sea level. The topographic profile along the line (not to vertical scale) is shown at the top. There is a 37-m elevation difference between Atexcac and Alchichica lakes. LD Las Derrumbadas rhyolitic extrusives. AT Atexcac maar, AL Alchichica maar.

The topographic profile in **Figure 11** shows that there is a considerable elevation difference between Atexcac and Alchichica lakes. From the digital elevation model of Ryan et al. (2009) we obtain lake elevations of 2357 m for Atexcac (**Figure 12**),

Fig. 12. Atexcac maar looking toward the south. Given the 37-m elevation difference with respect to Alchichica lake we assume that a perched aquifer interacted with ascending magma to generate this explosion crater.

2320 m for Alchichica (**Figure 13**), 2344 m for La Preciosa, and 2337 for Quechulac. Alchichica is located in the lowest elevation of the basin, with an elevation difference of 37 m with respect to Atexcac; smaller but significant elevation differences also occur with the neighboring lakes of La Preciosa and Quechulac. This may indicate the main aquifer (Toba Café) is fragmented, establishing various phreatic levels in the region. However, the elevation of Atexcac with respect to the other three maar lakes indicates this may be a different aquifer system, perhaps a perched

aquifer, also contributing to maar formation. Carrasco-Núñez et al. (2007) reported that almost no Toba Café is present in the tuff ring deposits of this maar, which is not surprising given the altitude difference of ~37 m between Atexcac lake and Alchichica, La Preciosa and Quechulac lakes, in which the Toba Café formation is present.

Fig. 13. Alchichica maar. In the foreground evaporites by the lake shore. In the background Las Derrumbadas rhyolitic domes.

6. Discussion

Geophysical studies on maar volcanism apparently have concentrated on elucidating the subsurface morphology of the diatremes, from which eruptive histories can be inferred (Montesinos et al. 2006; López-Loera et al. 2008; Blaikie et al. 2015; van den Hove et al. 2015). However, on the morpho-tectonic setting one finds considerably less works (Martín-Serrano et al. 2009; Cassidy and Locke, 2010); the present study pertains to this latter category, since we aimed at characterizing a single, large intrusive above which there are maars, cinder cones, lava flows and tuffs. We submit that these eruption centers were generated by the discrete ascent of magma from this intrusive.

In the above presentation of the 2-D models and the 3-D inversions we showed that a large intrusive characterized by a high magnetic susceptibility (~0.008 SI) and a large density (~2.9 g/cm^3) reproduces the regional, observed magnetic and gravimetric anomalies. Which suggest a causal relationship between the volcanic products observed on the surface and the distribution of the denser formations in the subsurface. This is in line with the observation of Blaikie et al. (2015) regarding eruptions in monogenetic fields, which are usually spatially and temporally linked. In **Figure 2** we showed the alignment of explosion craters, extrusive rhyolites, and cinder cones which correlate with the regional fault that also shows in the inverted model shown in **Figure 10a**. Similar linkages have been suggested for adjacent vents derived from aeromagnetic analyses. (Cassidy and Locke, 2010).

In **Tables 1 and 2** we summarized the surface volume calculations performed on individual volcanic structures of the study area. We first defined a surface for each structure which is used as a reference in the Digital Elevation Model (DEM) used (Ryan et al. 2009). This is a flat surface at a

given elevation, which was assumed to be undisturbed prior to the corresponding eruption (i.e., the country rock). In order to choose adequate reference surfaces we observed neighbouring flat areas that appeared undisturbed; thus we fixed the elevation of each reference surface. With the DEM of 20 m resolution we evaluated the volume above the surface which we attribute to ejecta from the eruption. We observed that the ejecta range can be well defined by variations in terrain elevation from the DEM, which in turn defined the area in which volumes would be evaluated. We also determined the volume under the reference surface which is directly linked to the excavation produced by the volcanic explosion. Where a lake exists its elevation is the limit of the excavation depth in the lake region. If the reference surface elevation is changed the corresponding volumes will vary accordingly. If the resolution (20 m) of the DEM is changed the volumes will also vary. In almost all instances the areas evaluated included geologic formations other than tephra. In those cases we performed corrections of the volume which in no case were larger than 10 percent and are included in the reported figures. The overall volume estimated error is ±8%.

For the case of Tecuitlapa maar we can compare our volume results with those reported by Ort and Carrasco-Núñez (2009). From Table 2 we obtain 0.069 km^3 for the ejecta and they report 0.056 km3 for the full maar-ring volume; the difference can be accounted for varying the elevation of the reference surface. They report crater volume below pre-existing surface as 0.019 km^3 while we obtain 0.039 km^3. It is worth noticing that they approximate a cylindrical geometry of 450 m radius and 30 m depth to the actual volume. Trying to reproduce this approximation we obtain from the DEM two diameters for the crater, an E-W diameter of 1300 m and a N-S diameter of 1050 m which averaged yield a radius of 587.5 m as well as two depths, one of 62 m from the top of the rim to the surface of the lake and another of 42 m from the reference surface (2420 m) to the surface of the lake. For the former depth the volume is 0.067 km^3, while for the latter the volume

is 0.045 km^3, which is closer to the 0.039 km^3 obtained without assuming a regular prism. It appears that the above authors underestimated the diameter and the depth of the excavated volume.

All of the above volume calculations are surface evaluations. Evaluating individual diatreme volumes is beyond the scope of this study, since it requires local geophysical measurements over each structure in order to have sufficient anomaly resolution (Blaikie et al. 2014; Cassidy et al. 2007). However, on the basis of the 3-D inversion results we can extract the subsurface volumes of the main anomalous bodies: Las Derrumbadas and the large intrusive associated with the main gravity and magnetic anomalies. In the inversion model used we can select density range and X, Y, Z ranges in which the volume is to be evaluated. The total volume will be given by the addition of all volume elements (voxels) that fulfil the selected criteria within the given boundaries. One must bear in mind that the inversion is performed up to a given defined depth; consequently the volumes can only be obtained to that depth.

Table 1. Ejecta and excavation volumes of selected structures in the north sector of the study area derived from the Digital Elevation Model (DEM) of Ryan et al. (2009). Elevation reference is the altitude of a flat surface assumed to exist before the corresponding structure was emplaced. Ejecta volume is the volume above the reference surface and excavation volume is the volume under that surface obtained from the DEM. Derr. Derrumbada; Tep. Tepeyehualco.

Structure Name	Type	Elevation Reference (m)	Lake Elevation (m)	Ejecta Volume (km^3)	Excavation Volume (km^3)
Alchichica	Maar	2340	2320	0.408	0.088
Preciosa	Maar	2350	2337	0.043	0.051

Quechulac	Maar	2350	2337	0.060	0.026
Atexcac	Maar	2397	2357	0.514	0.018
Tepexitl	Dry Crater	2417	----	0.061	0.001
Derr. SE	Dome	2400	----	9.786	----
Derr. NW	Dome	2400	----	9.486	----
Tep. Crater	Dry Crater	2340	----	2.372	----
Tep. Crater	Dry Crater	2417	2417*	1.219**	----
Tep. Dome	Dome	2340	----	4.306	----

*The lake is present in the rainy season and then evaporates.

**This volume corresponds mostly to tephra forming the rim of the crater.

The density range chosen for the evaluation of both subsurface bodies is 2.74 to 2.99 g/cm^3, which approximates the densities defined in the 2-D model for those intrusives (see **Figure 7 and Figure 10**). In the case of Las Derrumbadas the depth ranges from 2400 to -3760 m, where the negative number indicates below sea level. The volume obtained is 88.5 km^3. For the large intrusive the depth ranges from 1820 to -3760 m, since it does not reach to the surface. The volume obtained is 395.5 km^3. If a finer mesh is used for the inversion the accuracy will be increased. If the density range is varied the volumes will vary accordingly.

Calculating the volumes of these bodies using the magnetic susceptibility inversion results in the range of 1.6-7.1 x 10 $^{-5}$ SI (see **Figure 8a**) for the same depth ranges as for the density, we obtain a volume for Las Derrumbadas 171.5 km^3 and for the intrusive 470.7 km^3. Thus Las Derrumbadas volume changes ~90 percent between the density and susceptibility estimates, while the large

intrusive varies only ~20 percent. These variations are not surprising since two different physical properties are being evaluated and their distributions do not necessarily directly correspond to each other; in fact these differences potentially may shed light on the temperature conditions of the intrusives, although this possibility will be analysed in a different study.

Table 2. Ejecta and excavation volumes of selected structures in the south sector of the study area derived from the DEM of Ryan et al. (2009). Same definitions as in Table 1.

Structure Name	Type	Elevation Reference (m)	Lake Elevation (m)	Ejecta Volume (km^3)	Excavation Volume (km^3)
Tecuitlapa	Maar	2420	2377	0.069	0.039
Aljojuca	Maar	2419	2357	0.208	0.035
X. Grande	Dry crater	2500	----	0.127	0.024
X. Chico	Dry crater	2540	----	0.143	0.033
Zotoltepec	Scoria Cones	2505	----	0.242	----
Tecuitlapa	Volcano	2352	----	2.476	----

6. Conclusions

This study focused on characterizing an intrusive suspected to be the source of large magnetic and gravity anomalies, which gives rise on the surface to a group of maars, domes, lava fluxes, and tuffs. A nearby volcanic region to the south also contains this type of manifestations although it is

separated from the former by an area in which there are no volcanic manifestations. The northern region extends from Las Derrumbadas domes to Alchichica maar and encompasses the majority of the explosion craters in the area. A positive, circular magnetic anomaly in the region of lowest topography coincides with a positive gravity anomaly suggesting the underground presence of an intrusive with high density and high magnetic susceptibility. The gravity and magnetic models confirm its presence. The models show the proximity of the intrusive to the surface, which presumably heats up the aquifers contained in the Toba Café formation, inducing explosions and creating maars. 2-D gravity and magnetic models, plus one cross-section obtained from the gravity field inversion independently confirm that projections of the main body towards the surface coincide with the location of the maars existing along the modeled lines. For this group we calculated the ejecta volumes from various structures which lie within the ranges observed in different volcanic settings. We noted that the volume of the diatremes cannot be determined with the present dataset since it requires detailed geophysical measurements within each structure, which is beyond the objective of our study.

The southern source extends from Tecuitlapa to Xalapazco Grande and is more limited in extent and number of surface structures. Ejecta volumes were also calculated for this group. The magnetic inversion results indicate that it extends eastwardly from Tecuitlapa volcano structure, covering the surface area in which maars, dry explosion craters, and cinder cones appear along the E-W direction. In Tecuitlapa volcano magnetic models show the geometry of a thin volcanic feeder, also with a high magnetic susceptibility.

The 3-D inversion results represent a powerful tool for analyzing the distribution of specific densities or magnetic susceptibility values within the volume of the inversion that may lead to

structural definitions within the resolution of the inversion. This regional study will allow more detailed geophysical modeling of specific targets associated with each one of the intrusives identified.

Acknowledgements

The valuable comments of K. Németh and an anonymous reviewer greatly helped improve the original manuscript. In the field work we acknowledge the assistance of Nereida de la Paz Pérez Méndez.

References

Alvarez, R., Maupomé, L. and Tejera, A. 1976. Magnetic comparison of explosion craters and volcanic cones. Geofísica Internacional, 16, 63-94.

Alvarez, R., Yutsis, V., 2015. Southward Migration of Magmatic Activity in the Colima Volcanic Complex: An Ongoing Process. International Journal of Geosciences, Vol.6, No. 9, pp. 1077-1099

Alvarez, R., Corbo Camargo, F, Yutsis, V.V., 2017a. Geophysical modelling of Isla Isabel: a volcanic island on the Mexican continental margin. In: Németh, K., Carrasco-Núñez, G., Aranda-Gómez, J. J. & Smith, I. E. M. (eds.) Monogenetic Volcanism. Geological Society, London, Special Publications, 446, 295-310, 3 March, 2017

Alvarez, R., Corbo Camargo, F., Yutsis V.V., Arzate, J.A., 2017b. A volcanic centre in Mexico's Pacific continental shelf. In: Németh, K., Carrasco-Núñez, G., Aranda-Gómez, J. J. & Smith, I. E. M. (eds.) Monogenetic Volcanism. Geological Society, London, Special Publications, 446, No.1, pp. 281-293. First published online March 3, 2017

Austin-Erickson, A., Ort M.H., Carrasco-Núñez, G. 2011. Rhyolitic phreatomagmatism explored: Tepexitl tuff ring (Eastern Mexican Volcanic Belt). J. Volc. Geoth. Res., 201, 301-341.

Baranod, V. and Naudy, H. 1964. Numerical calculation of the formula of reduction to the magnetic pole. Geophysics. 29, 67-79

Bazán, S., 1959. Geological survey to perform a terrain classification in the NW portion of the Oriental-Serdán basin, States of Puebla and Tlaxcala. Professional Thesis (In Spanish, unpublished). 53p. Escuela Superior de Arquitectura. Instituto Politécnico Nacional.

Blaikie, T.N., Ailleres, L., Betts, P.G. and Cas, R.A.F., 2014. Interpreting subsurface volcanic structures using geologically constrained 3-D gravity inversions: Examples of maar-diatremes, Newer Volcanics Province, southeastern Australia. Journal of Geophysical Research. Solid Earth, 119(4), 3857-3878.

Blaikie, T.N., van Otterloo, J., Ailleres, L., Betts, P.G., and Cas, R.A.F., 2015. The erupted volumes of tephra from maar volcanoes and estimates of their VEI magnitude: Examples from the late Cenozoic Newer Volcanics Province, south-eastern Australia. Journal of Volcanology and Geothermal Research 301, 81-89.

Campos-Enriquez, J. and Garduno-Monroy, V.H., 1987. The shallow structure of Los Humeros and Las Derrumbadas geothermal fields, Mexico. Geothermics, 16(5-6), 539-554.

Carrasco-Núñez, G., Ort, M. H, and Romero, C. 2007. Evolution and hydrological conditions of a maar volcano (Atexcac crater, Eastern Mexico). Jour. Volc. Geotherm. Res. 159, 179–197. doi:10.1016/j.jvolgeores.2006.07.001

Cassidy, J., France, S.J., Locke, C.A., 2007. Gravity and magnetic investigation of maar volcanoes, Auckland volcanic field, New Zealand. Journal of Volcanology and Geothermal Research 159 (1-3), 153-163

Cassidy, J., Locke C.A., 2010. The Auckland volcanic field, New Zealand: Geophysical evidence for structural and spatio-temporal relationships. Journal of Volcanology and Geothermal Research, 195, 127-137

Ellis, R.G., de Wet, B. and Macleod, I.N., 2012. Inversion of magnetic data for remnant and induced sources, Australian Society of Exploration Geophysicists, Extended Abstracts 2012, 1-4. Melbourne, Australia.

Ferrari, L., Garduño, V., Pasquaré, G., Tibaldi, A., 1991, Geology of Los Azufres caldera, Mexico, and its relations with regional tectonics: Journal of Volcanology and Geothermal Research, 47, 129-148

Ferrari, L., Tagami, T., Eguchi, M., Orozco-Esquivel, M. T., Petrone, C., Jacobo-Albarrán, J., López-Martínez, M., 2005. Geology, geochronology and tectonic setting of late Cenozoic volcanism along the southwestern Gulf of Mexico: the Eastern Alkaline Province revisited. Journal of Volcanology and Geothermal Research, 146, 284-306.

Ferriz, H. and Mahood, G.A., 1986. Volcanismo riolítico en el Eje Neovolcánico Mexicano. Geof. Int. Vol. 25- I, pp. 117-156.

Geyer, A. and Martí, J., 2010. The distribution of basaltic volcanism on Tenerife, Canary Islands: Implications on the origin and dynamics of the rift systems. Tectonophysics, 483(3-4), 310-326

Gómez-Tuena, A. y Carrasco-Nuñez, G. 2000. Cerro Grande volcano: the evolution of a Miocene stratocone in the early Trans-Mexican Volcanic Belt. Tectonophysics 318, 249-280

Gutiérrez-Negrín, L.C.A. 2015. Mexican Geothermal Plays. Proceedings World Geothermal Congress. Melbourne, Australia, 19-25 April 2015

Lira, H. 2005. Actualización del modelo geológico conceptual del campo geotérmico del Cerro Prieto. Geotermia, 18(1), 37-46.

López-Loera, H., Aranda-Gómez, J.J., Arzate, J.A., Molina-Garza, R.S., 2008. Geophysical surveys of the Joya Honda mar (México) and surroundings; volcanic implications. Journal of Volcanology and Geothermal Research, 170, 135-152.

Lorenz, V., 1986. On the growth of maars and diatremes and its relevance to the formation of tuff rings. Bulletin of Volcanology, 48 (5), 265-274.

Macleod, I.N. and Ellis, R.G., 2013. Magnetic vector inversion, a simple approach to the challenge of varying direction of rock magnetization, Australian Society of Exploration Geophysicists, Extended Abstracts 2013, 1-4, Melbourne, Australia.

Martín-Cerrano, A., Vegas, J., García-Cortés, A., Galán, L., Gallardo Millán, J., Martín-Alfageme, S., Rubio, F.M., Ibarra Torre, P.I., Granda, A., Pérez-González, A., García-Lobón, J.L., 2009. Morphotectonic setting of maar lakes in the Campo de Calatrava Volcanic Field (Central Spain, SW Europe). Sedimentary Geology 222(1-2), 52-63. DOI: 10.1016/j.sedgeo.2009.07.005

Maupomé, L., Alvarez, R., Kieffer, S.W., and Dietz, R.S., 1975. On the terrestrial origin of Tepexitl crater, Mexico. Meteoritics, 10, 209-214.

Montesinos, F. G., J. Arnoso and R. Vieira, 2005. Using a genetic algorithm for 3-D inversion of gravity data in Fuerteventura (Canary Islands), Int. J. Earth Sci., 94: 301-316. Montesinos, F.G.,

Arnoso, J., Benavent, M., Vieira, R., 2006. The crustal structure of El Hierro (Canary Islands) from 3-D gravity inversion, J. Volcanol. and Geotherm. Res. 150/1-3 pp 283-29

Mrlina, J., Kämpf, H., Kroner, C., Mingram, J., Stebich, M., Brauer, A., Geissler, W.H., Kallmeyer, J., Matthes, H., Seidl, M., 2009. Discovery of the first Quaternary maar in the Bohemian Massif, Central Europe, based on combined geophysical and geological surveys. Journal of Volcanology and Geothermal Research 182 (2009) 97–112

NAMAG 2002. North American Magnetic Anomaly Group. Magnetic Anomaly Map of North America. US Department of the Interior and US Geological Survey. Scale 1:10000000

Németh, K., Kereszturi, G., Agustin-Flores, J., Briggs, R., Cronin, S.J., Lindsay, J.M., Pittari, A., Smith, IEM 2012. Monogenetic volcanism of the South Auckland and Aucklend Volcanic Fields. Field Guide, 4th International Maar Conference, Aucklend, New Zealand, Geoscience Society of New Zealand Miscellaneous Publication 131B.

Ordóñez, E., 1906. Xalapaxcos of Puebla State (In Spanish). Parergones del Instituto de Geología, México. V. 1, 295-393.

Ort, M. and Carrasco-Nuñez, G. 2004. Vent alignments of maar volcanoes. Occasional papers of the Geological Institute of Hungary. Abstract volume of the Second International Maar Conference, 203. p82.

Ort, M.H. and Carrazco-Nuñéz, G. 2009. Lateral vent migration during phreatomagmatic and magmatic eruptions at Tecuitlapa Maar, east-central Mexico. Journal of Volcanology and Geothermal Research 181(1):67-77. DOI: 10.1016/j.jvolgeores.2009.01.003

Ort, M.H. and Carrazco-Nuñéz, G. 2014. Phreatomagmatism in the Serdán-Oriental Basin, Eastern Mexican Volcanic Belt. IAVCEI – 5IMC, Querétaro, México, pp.12-13

Paoletti, V., Di Maio, R., Cella, F., Florio, G., Motschka, K., Roberti, N., Secomandi, M, Supper, R., fedi, M., Rapolla, A., 2009. The Ischia volcanic island (Southern Italy): Inferences from potential field data interpretation. Journal of Volcanology and Geothermal Research 179, 69–86

Prol, R.M., González-Moran, T., 1982. Modelo preliminar del régimen térmico conductivo en la caldera de Los Humeros, Puebla. Geof. Int., Vol. 21 (3), 295-307

Riggs, N. and Carrasco-Nuñez , G., 2004. Evolution of a complex, isolated dome system, Cerro Pizarro, central Mexico. Bull. Volcanol. 66, 322-335.

Ryan, W. B. F., Carbotte, S.M., Coplan, J.O., O'Hara, S., Melkonian, A., Arko, R., Weissel, R.A., Ferrini, V., Goodwille, A., nitsche, F., Bonczkowski, J, Zemsky, R. 2009. Global multi-resolution topography synthesis. Geochemistry, Geophysics, Geosystems, 10, Q03014, doi:10.1029/2008GC002332.

Siebe, C., and Verma, S.P., 1988. Major element geochemistry and tectonic setting of Las Derrumbadas rhyolitic dome, Puebla, Mexico. Chem. Erde, 48 (3), 177- 189.

Valentine, G.A., White, J.D.L., Ross, P.-S., Amin, J., Taddeucci, J., Sonder, I., and Johnson, P.J., 2012. Experimental craters formed by single and multiple buried explosions and implications for volcanic craters with emphasis on maars. Geophysical Research Letters, Vol. 39, L20301, doi:10.1029/2012GL053716, 2012

Van den Hove, J.C., Ailleres, L., Betts, P,G,, Cas, R.A.F., 2015. Subsurface structure of a large basaltic maar volcano examined using geologically constrained potential field modelling, Lake Purrumbete

Maar, Newer Volcanics Province, southeastern Australia. *Journal of Volcanology and Geothermal Research* 304, 142-159.

Whiting, T.H., 1986. Aeromagnetics as an aid to geological mapping - a case history from the Arunta Inlier, Northern Territory. Australian Journal of Earth Sciences, 33, 271 - 286.

Yáñez, C. and Casique-Vázquez, J. 1980. Geothermal Project Los Humeros-Derrumbadas. Geological Report. 59p. (In Spanish, unpublished). Comisión Federal de Electricidad, México DF.

Highlights:

- Potential fields modeling (2D and 3D inversion) was applied to Serdán Oriental basin, Eastern Mexico
- Joint interpretation of gravity and aeromagnetic data focused on characterizing an intrusive suspected to be the source of large magnetic and gravity anomalies, which gives rise on the surface to a group of maars, domes, lava fluxes, and tuffs.
- The models show the proximity of the intrusive to the surface, which presumably heats up the aquifers contained in the Toba Café formation, inducing explosions and creating maars.